scientific reports

Check for updates

OPEN

# A novel cancer-associated membrane signature predicts prognosis and therapeutic response for lung adenocarcinoma

Biao Tu[1,2], Jun Wu[2,3]✉, Wei Zhang[3], Haitao Tang[1], Tenghui Dai[3] & Bingfeng Xie[1]✉

**Lung adenocarcinoma (LUAD) is a leading cause of cancer-related death, and reliable biomarkers for prognosis and treatment guidance remain limited. Membrane proteins play key roles in tumor progression and therapeutic response, yet their clinical utility in LUAD remains underexplored. We integrated scRNA-seq, spatial transcriptomics, and bulk RNA-seq datasets from multiple LUAD cohorts to identify cancer-specific membrane proteins derived from epithelial subpopulations. Based on these results, we constructed a prognostic signature, LCaMPS, and evaluated its predictive performance using multiple datasets. The expression of model genes was confirmed at both the bulk RNA and protein levels. Associations with the tumor microenvironment (TME) and drug sensitivity were further analyzed. A distinct LUAD-enriched epithelial cluster (Epi_c0) exhibiting hypoxic and EMT signatures was identified. 35 cancer-specific membrane proteins were defined, several of which, including TSPAN8, BACE2, and COX16, showed strong spatial localization within the tumor regions. LCaMPS, a 9-membrane gene-based prognostic model, stratified patient prognosis and predicted 5- and 10-year survival rates with high accuracy. High LCaMPS scores were associated with increased infiltration of neutrophils, endothelial cells, and fibroblasts in the TME and predicted higher sensitivity to 66 chemotherapeutic agents, including Gemcitabine and Sorafenib. Low-risk patients were predicted to respond better to drugs, such as Cisplatin and Parthenolide. This study highlights the importance of membrane expression patterns in LUAD at single-cell and spatial resolution. The LCaMPS model provides a robust prognostic and therapeutic stratification tool with potential applications in personalized cancer management.**

**Keywords** Membrane, scRNA-seq, Spatial transcriptomics, Prognosis, Lung adenocarcinoma

Lung cancer remains the leading cause of cancer-related mortality worldwide[1]. Non-small cell lung cancer (NSCLC) constitutes the predominant pathological subtype, with lung adenocarcinoma (LUAD) accounting for approximately 40% of all lung cancer cases[2,3]. LUAD is characterized by a high incidence and mortality rate, and patients often present with advanced-stage disease, resulting in poor clinical outcomes[4]. However, the 5-year overall survival (OS) rate in patients with LUAD is less than 20%[5]. Therefore, it is necessary to develop novel prognostic biomarkers and individualized therapeutic strategies to improve patient outcomes.

Over the past decade, the advent of single-cell RNA sequencing (scRNA-seq) and emerging spatial transcriptomics technologies has enabled high-resolution dissection of LUAD tumorigenesis and progression at both the cellular and spatial levels[6–9]. scRNA-seq has revealed critical insights into LUAD cell differentiation trajectories, tumor microenvironment (TME) composition, and cellular reprogramming[6–8].

Membranes play pivotal roles in cellular processes such as membrane transport, cell migration, programmed cell death, and autophagy[10]. Membrane dysregulation can lead to enhanced tumor cell proliferation, survival, invasion, and metastasis[10]. Notably, silencing specific membranes has been shown to suppress tumor invasion and metastasis[11].

While scRNA-seq captures the transcriptional diversity of individual cell populations, spatial transcriptomics provides spatially resolved gene expression profiles within tumor tissue[9,12]. Despite these advances, there is still

[1]Department of Cardiothoracic Surgery, The First Hospital of Changsha, Changsha 410005, Hunan Province, China. [2]School of Biomedical Science, Hunan University, Changsha 410082, Hunan Province, China. [3]Institute for Brain Research and Rehabilitation, South China Normal University, Guangzhou 510631, China. ✉email: bioinfo1695@163.com; xbfiuy@126.com

a lack of LUAD prognostic models that integrate the cancer-relevant features of membranes derived from single-cell and spatial transcriptomic data.

We hypothesized the existence of a distinct epithelial subpopulation in LUAD, characterized by the expression of cancer-specific membranes, which may serve as potential prognostic and therapeutic biomarkers. Here, we integrated scRNA-seq, spatial transcriptomics, and bulk RNA-seq data to identify LUAD-specific membranes and to construct a prognostic model, LCaMPS. We further validated the model and assessed its associations with TME and predicted drug response, aiming to provide insights into precision oncology for LUAD.

## Materials and methods

### Data collection

This study included 4 LUAD-related scRNA-seq cohorts: GSE117570[8], GSE131907[7], GSE164983, and GSE274934[6] with a total of 37 samples (15 adjacent normal (ADJ) tissues and 22 LUAD tissues). The spatial transcriptomic data were obtained from the HTAN cohort with 3 LUAD slices. And bulk RNA-seq data were retrieved from the TCGA-LUAD cohort ($n = 575$), as well as from the GEO datasets GSE26939 ($n = 115$)[13] and GSE72094 ($n = 398$)[14]. Detail sample information can be found in supplementary table S1 and S2.

### Data quality control and processing

For bulk RNA-seq data, the downloaded LUAD expression matrix was converted from Ensemble IDs to gene symbols. In cases of duplicated gene symbols, the mean expression value was taken to obtain a standardized gene expression matrix for downstream analysis. For scRNA-seq data, the 4 cohorts were merged using Seurat[15]. Cells with nCount < 1000, nCount > 100,000, nFeature < 500, nFeature > 10,000, and mitochondrial percentage (pMT) > 10% were filtered out. Data normalization, dimensionality reduction, and clustering were then performed. Batch effects were removed using Harmony to generate a scRNA-seq atlas for downstream analysis[16]. For spatial transcriptomics, data normalization was carried out using spatialPreprocess from BayesSpace[17]. The appropriate number of clusters was selected using qTune, and spatial clustering was performed with spatialCluster. All analyses were conducted in R version 4.4.1.

### Annotation of cellular populations

For the 18 clusters generated by Seurat from the scRNA-seq atlas, cell type annotation was based on CellMarker 2.0 and marker genes reported in previous studies[7,18]. After removing doublet or undetermined clusters, a total of 162,193 cells were categorized into 8 major cell types. The major cell types were identified based on canonical markers, including *PTPRC* for immune cells; *CD79A*, *MS4A1*, and *IGHA2* for B cells; *CD3E*, *CD3D*, *CD3G*, and *TRAC* for T cells; *PECAM1*, *VWF*, and *CLDN5* for endothelial cells; *EPCAM*, *KRT18*, and *KRT19* for epithelial cells; *COL1A1*, *DCN*, and *COL1A2* for fibroblasts; *CD68*, *MARCO*, and *LYZ* for myeloid cells; *CPA3* and *KIT* for mast cells; and *NKG7*, *GNLY*, and *KLRD1* for natural killer (NK) cells.

And the spatial transcriptomics data, each of the 3 LUAD tissue sections was independently subjected to spatial clustering, resulting in 8 spatial clusters comprising a total of 6,315 spots.

### Differential expression gene analysis

For the epithelial cell cluster in the scRNA-seq atlas, highly expressed genes were identified using Seurat's FindAllMarkers function with the parameters test.use = "wilcox", only.pos = TRUE, logfc.threshold = 0.25, and min.pct = 0.25. The results were visualized using pheatmap. Differential gene expression between LUAD and adjacent normal (ADJ) samples was analyzed using the FindMarkers function with parameters test.use = "wilcox", only.pos = FALSE, and logfc.threshold = 0. The results were visualized using EnhancedVolcano.

For differential expression analysis between high- and low-risk LCaMPS groups, DESeq2 was used with default parameters, and the results were applied to downstream GSEA enrichment analysis.

### Spatial relationship analysis

Spatial enhancement of spots was performed using spatialEnhance from BayesSpace. The enhanceFeatures function was applied to enhance the spatial expression of genes associated with tumor, cancer-specific membrane, and LCaMPS signatures. Detailed information on the signature genes can be found in supplementary table S3. Pearson correlation coefficients were used to evaluate spatial correlations between features, and the results were visualized using ggscatter.

### Protein-protein interaction network analysis

The protein–protein interaction (PPI) network of the 37 cancer-specific membrane proteins was predicted using the STRING database with the species parameter set to *Homo sapiens* and other parameters left as default[19]. The PPI network was further refined and visualized in Cytoscape for better presentation. Functional pathway enrichment results derived from the PPI network were visualized using ggplot2.

### Construction and validation of the prognostic model

The prognostic value of the 37 LUAD cancer-specific membrane genes for OS in LUAD patients was assessed using univariate Cox regression analysis based on the TCGA-LUAD cohort. Membrane genes with a $p$-value < 0.05 and hazard ratio (HR) > 1 were selected as input features for least absolute shrinkage and selection operator (LASSO) regression. The optimal set of prognostic features was identified using LASSO with 10-fold cross-validation, and non-zero coefficients were extracted for each selected gene. A LUAD cancer-associated membrane prognosis signature (LCaMPS) was then constructed based on the expression levels of these genes and their corresponding risk coefficients (supplementary table S4). Patients were stratified into high-risk and low-risk groups according to the median risk score. The formula for calculating the LCaMPS risk score is as follows:

$$LCaMPS = \sum_{i=1}^{k} mRNA\,expression\ (i) * risk\,coefficient\ (i)$$

To evaluate the prognostic performance of LCaMPS, statistical significance was determined using the log-rank test, and Kaplan–Meier survival curves were generated. The R package timeROC was used to calculate the area under the curve (AUC), and ggplot2 was applied to visualize the receiver operating characteristic (ROC) results. The predictive power of the model was further validated by AUC and Kaplan–Meier analyses in two independent external cohorts, GSE26939 and GSE72094.

### Functional analysis

Enrichment analysis of the 7 epithelial cell clusters was performed using the hallmark gene sets from the molecular signatures database (MSigDB)[20]. Gene set variation analysis (GSVA) with the method set to "ssgsea" was used to compute the single-sample gene set enrichment analysis (ssGSEA) scores for all 50 Hallmark pathways across the 7 epithelial clusters. The results were visualized using pheatmap. For functional enrichment analysis of the LCaMPS model, the fgsea package was applied to assess kyoto encyclopedia of genes and genomes (KEGG)[21,22] pathway gene sets from MSigDB, and the results were visualized using ggplot2.

### Tumor microenvironment and infiltration analysis

To evaluate the impact of the LCaMPS score on stromal and immune cell infiltration in the tumor microenvironment (TME), we applied ESTIMATE, MCP-counter[23]and CIBERSORT[24] to calculate infiltration scores for different cell types. Patients were stratified into high- and low-risk groups based on the median LCaMPS score. The Wilcoxon test was used to assess the statistical significance of differences between groups. The results from ESTIMATE, MCP-counter, and CIBERSORT were visualized separately using ggplot2.

### Protein expression of LCaMPS signatures

Immunohistochemistry (IHC) data for the 8 LCaMPS signature proteins were retrieved from The Human Protein Atlas (THPA) online database[25]. IHC images of LUAD tissues and corresponding normal lung tissues for each of the 8 signatures were selected, integrated, and visualized. As THPA does not provide protein expression data for PMEPA1, only 8 out of the 9 LCaMPS signature proteins were visualized in this study. The staining intensity was categorized by the THPA into four levels: not detected, low, medium, and high. IHC staining information for all analyzed genes in both LUAD and normal lung tissues can be accessed directly from the THPA database.

### Anti-tumor drug therapeutic response analysis

To assess whether there are differences in the predicted treatment response to different drugs between LCaMPS high-risk and low-risk groups, the R package pRRophetic v0.5 was used to predict drug sensitivity based on mRNA expression matrices of tumor samples from the TCGA-LUAD dataset[26]. The function pRRopheticPredict was used with the parameters set as follows: tissueType = "all", dataset = "cgp2014". A total of 138 drugs were evaluated, and the results were visualized using ggpubr. Detailed significant results of the drug sensitivity analysis can be found in supplementary table S5.

### Statistical analysis

Where appropriate, differences between groups were calculated using either student t-tests or Wilcoxon tests, depending on the data distributions. Survival analysis was conducted using the log-rank test. A $p$-value $< 0.05$ was considered statistically significant. $^{*}p < 0.05$, $^{**}p < 0.01$, and $^{***}p < 0.001$.

## Results

### Single-cell and spatial transcriptomic landscape of LUAD

This study integrated multiple transcriptomic datasets of different types to identify a class of LUAD cancer-specific membranes and to construct a predictive signature for prognosis and therapeutic response evaluation (Fig. 1A). We first integrated and performed quality control on four scRNA-seq datasets comprising a total of 37 samples (15 ADJ and 22 LUAD tissues) (Figure S1A). Based on clustering and classical marker gene expression, 17 clusters were initially annotated. After removing undetermined cell types, eight major cell types were retained, encompassing 162,139 cells (Fig. 1B, S1B, and S1C). We compared the cell type proportions and densities between LUAD and ADJ tissues. Myeloid and NK cells were enriched in ADJ tissues, whereas T cells, B/plasma cells, and epithelial cells were more abundant in LUAD tissues. No significant differences were observed in fibroblasts or mast cells (Fig. 1C and D). Marker gene expression showed clear specificity across cell types, for instance, *EPCAM* and *KRT8* were specifically expressed in epithelial cells, whereas all immune cells expressed *PTPRC* ($CD45^{+}$) (Fig. 1E). Furthermore, spatial transcriptomic profiling of the 3 LUAD tumor tissues identified 8 spatial clusters covering a total of 6,315 spots (Fig. 1F). Thus, these datasets constitute a comprehensive scRNA-seq atlas and spatial transcriptomic map that serve as a foundation for subsequent analyses.

### Identification of LUAD tumor-specific epithelial cluster

To investigate epithelial cell specificity in LUAD, epithelial cells were subsetted and cells expressing non-epithelial markers were removed. After re-clustering and dimensionality reduction, 7 epithelial cell clusters comprising 12,287 cells, were identified (Fig. 2A). Compared to ADJ tissues, the epi_c0 cluster exhibited a higher proportion and cell count in LUAD samples (Fig. 2A and B). Notably, epi_c0 was consistently present in 17 of 22 LUAD samples (Figure S2A). Differential gene expression analysis revealed that *TCIM*, *TENT5A*, *CAMK2N1*, and *HP* were highly expressed in the epi_c0 cluster (Fig. 2C). This cluster was enriched in apoptosis, epithelial-mesenchymal transition (EMT), hypoxia, and the p53 signaling pathway (Fig. 2D). Genes such as *TCIM* and

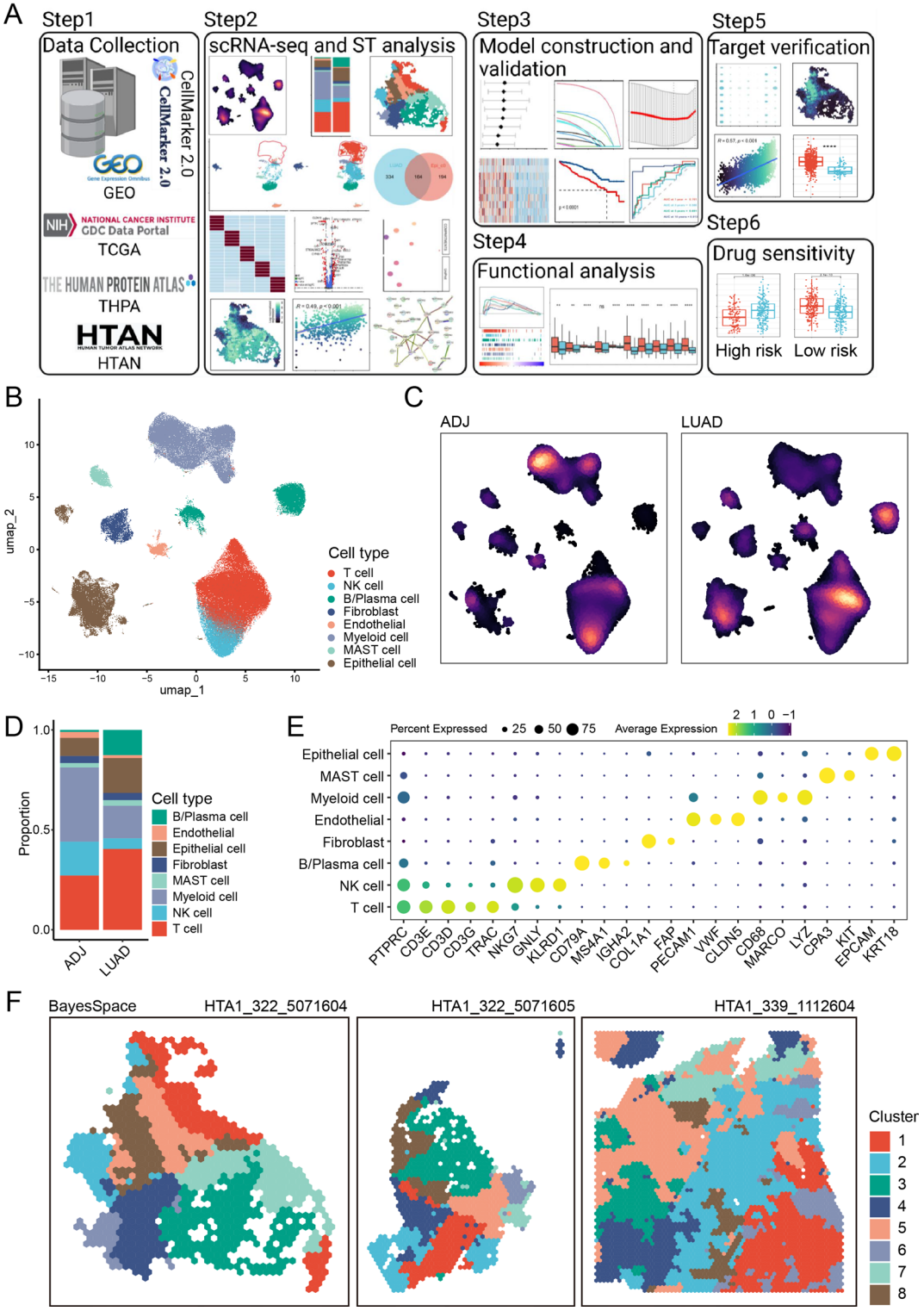


**Fig. 1**. Workflow and landscape of this study. (**A**) Workflow of this study. (1) Data were downloaded from public databases, including GEO, TCGA, HTPA, HTAN, and CellMarker 2.0. (2) Cancer-associated membrane genes were identified through single-cell RNA sequencing and spatial transcriptomics analysis. (3) The prognostic model was constructed based on the TCGA-LUAD cohort and evaluated using independent external datasets. (4) Functional analysis of the model was performed. (5) Verification of model signature genes. (6) Analysis of therapeutic drug sensitivity. (**B**) UMAP plot showing 8 major cell types, with different colors distinguishing cell types. (**C**) UMAP plot illustrating the density distribution of cell types in adjacent (ADJ) and LUAD tissues. The color gradient from dark to bright represents increasing density. (**D**) Box plot showing the proportion of different cell types in ADJ and LUAD tissues. Colors are consistent with (**B**). (**E**) Bubble plot displaying the expression levels of marker genes across the 8 cell types. (**F**) Spatial plot showing the spatial clustering of three LUAD tissue samples, with 8 clusters identified by BayesSpace.

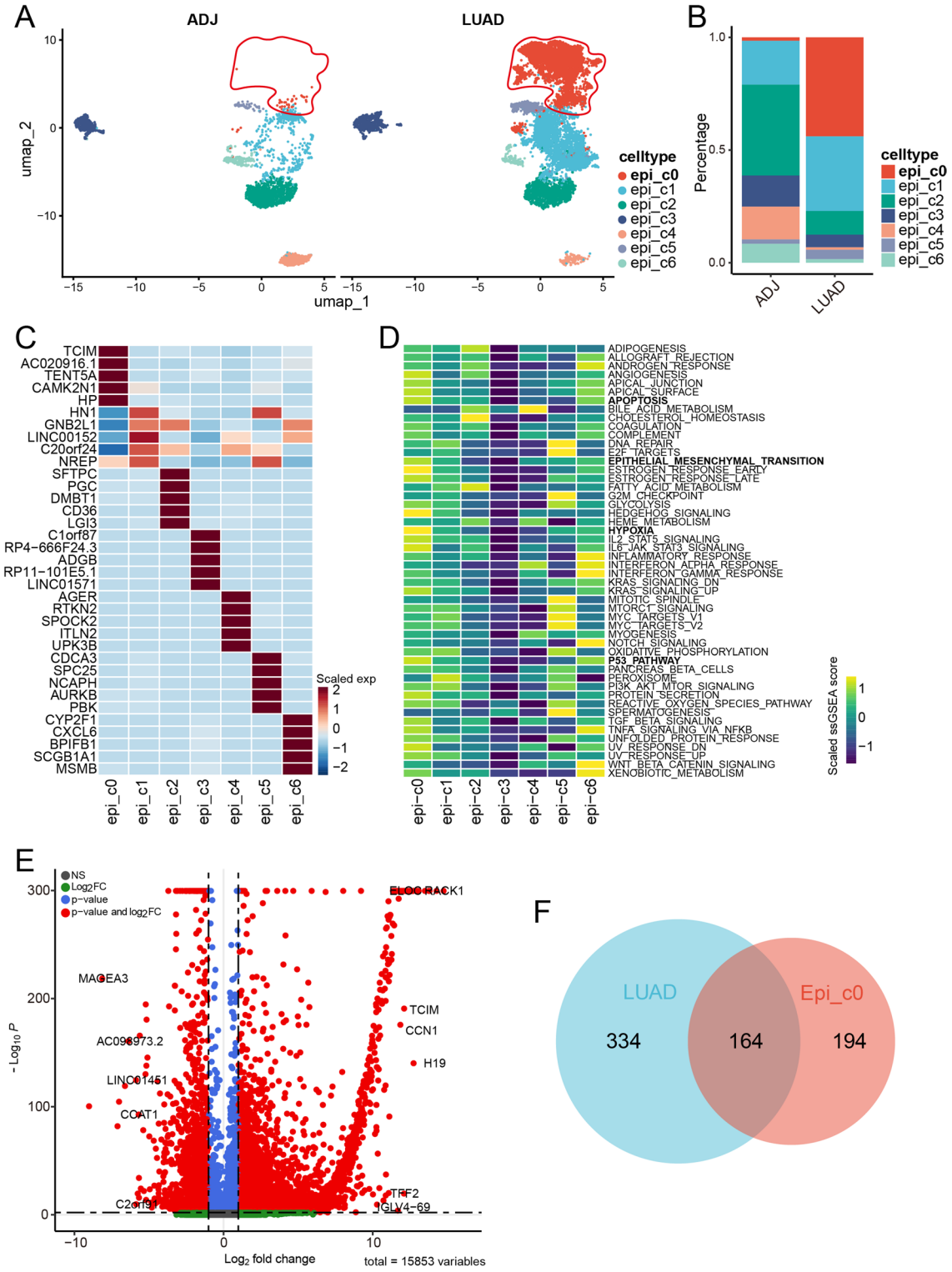


**Fig. 2**. Identification of tumor-specific epithelial cell clusters in LUAD. (**A**) UMAP plot illustrating 7 epithelial cell clusters in ADJ and LUAD tissues. (**B**) Barplot depicting the proportions of 7 epithelial cell clusters in ADJ ($n = 15$) and LUAD ($n = 22$) tissues. (**C**) Heatmap illustrating the expression of the top 5 genes in 7 epithelial cell clusters. (**D**) Heatmap showing the ssGSEA score of 50 hallmark pathways across 7 epithelial cell clusters. (**E**) Volcano plot of DEGs in epithelial cells between LUAD and ADJ tissues. (**F**) Venn plot illustrating the intersection of highly expressed genes in LUAD and those highly expressed in epithelial cell cluster c0.

*CCN1*, which were highly expressed in epi_c0, also showed elevated expression in the LUAD tissues (Fig. 2E). Furthermore, 164 genes overlapped between those that were highly expressed in LUAD tissues and epi_c0 cells (Fig. 2F). Taken together, these results identified a LUAD-specific epithelial cell cluster characterized by the expression of tumor-associated genes and enriched in cancer-relevant functional pathways.

## Characterization of LUAD epithelial-specific membranes

Given the critical role of membrane proteins in tumor progression[27]we identified 98 membrane genes that were significantly upregulated in LUAD compared to that in ADJ tissues out of 923 candidates (Fig. 3A). Moreover, 35 of these LUAD-upregulated membrane genes overlapped with genes specifically overexpressed in the LUAD-specific epithelial cluster epi_c0 (Fig. 3B). These overlapping genes, including *COX16*, *PLAUR*, *PLOD1*, *PLOD2*, *BACE2*, *SLC16A3*, *TSPAN8*, *IFITM1*, *and VIM*, were referred to as cancer-specific membranes (Fig. 3B). Spatial transcriptomic analysis revealed that the expression and localization of these cancer-specific membranes were strongly associated with LUAD tumor regions (Pearson correlation coefficients $R = 0.49$ in the HTA1_332_5071604 sample, and $R = 0.42$ in HTA1_332_5071605, while it was below 0.1 in HTA1_339_1112604, $p < 0.001$) (Fig. 3C and S2B). Subsequently, a PPI network revealed direct or indirect interactions among 15 genes, including *TSPAN8*, *VIM*, *PLAUR*, *IER3*, and *IFITM1* (Fig. 3D). In particular, *PLOD1* and *PLOD2* showed direct interaction (Fig. 3D). Functional enrichment of the PPI network indicated membrane-related functions and extracellular space components (Fig. 3E). Interestingly, glycoproteins were enriched within this PPI network, including *BACE2*, *PLAUR*, *VIM*, *IER3*, *PLOD1*, and *PLOD2* (Fig. 3E and S2C). These findings suggest that membranes specifically expressed in LUAD epithelial clusters are closely associated with tumor spatial localization and extracellular functional roles, with a notable porportion classified as glycoproteins.

## Construction and validation of the LCaMPS

To further investigate the prognostic potential of LUAD-specific epithelial membranes, we selected 35 candidate membrane genes and performed univariate Cox regression analysis in the TCGA-LUAD cohort. 13 membrane genes were significantly associated with poor OS (Fig. 4A). LASSO regression was then applied to determine the optimal predictive model (Fig. 4B). This process yielded a lung cancer-associated membrane prognosis signature (LCaMPS) consisting of 9 genes with nonzero coefficients (Table S4). The patients were stratified into high- and low-risk groups based on the median LCaMPS score. The expression levels of the 9 LCaMPS genes were consistently higher in the high-risk group than in the low-risk group (Fig. 4C). In the TCGA cohort, LCaMPS effectively stratified patient prognosis, with a log-rank p-value < 0.0001 (Fig. 4D). The AUC for 1-, 3-, 5-, and 10-year survival were 0.640, 0.688, 0.644, and 0.684, respectively (Fig. 4E). The model was further validated using the external dataset GSE72094 ($n = 398$), which also exhibited strong prognostic discrimination (log-rank $p < 0.0001$). The corresponding AUC values for 1-, 3-, 5-, and 10-year survival were 0.700, 0.617, 0.713, and NA, respectively (data not available) (Fig. 4F and G). Similarly, in the GSE26939 cohort ($n = 115$), the LCaMPS model demonstrated significant prognostic power (log-rank $p = 0.0011$), with AUC values of 0.701, 0.586, 0.691, and 0.913 for 1-, 3-, 5-, and 10-year survival, respectively (Fig. 4H and I). Collectively, these results indicate that the LCaMPS model offers valuable prognostic insight for patients with LUAD and holds potential for clinical application in risk stratification.

## Functional characterization of LCaMPS and its association with TME infiltration

Based on the median LCaMPS score, samples were stratified into high- and low-risk groups. GSVA analysis of KEGG pathways[21] showed that the high-risk group was significantly enriched in pathways related to tumor progression, including cell cycle ($p = 0.0256$, normalized enrichment score (NES) = 3.3), DNA replication ($p = 0.0018$, NES = 2.99), ECM-receptor interaction ($p = 0.0082$, NES = 2.9), mTOR signaling pathway ($p = 0.0024$, NES = 1.84), p53 signaling pathway ($p = 0.0047$, NES = 2.7), and non-small cell lung cancer ($p = 0.0034$, NES = 1.92 ; Fig. 5A). These results indicated that higher LCaMPS scores were associated with increased tumor cell proliferation and invasion. To explore the relationship between LCaMPS scores and the TME, we evaluated the infiltration of immune and stromal cells using 3 independent methods (Fig. 5). The ESTIMATE algorithm showed no significant difference in the immune score, stromal score, or tumor purity between the high- and low-risk groups (Fig. 5B). In contrast, the MCP-counter revealed significantly higher infiltration of myeloid-derived cells, including monocytic lineage cells, dendritic cells, and neutrophils, as well as endothelial cells and fibroblasts in the high-risk group (Fig. 5C). Similarly, CIBERSORT analysis showed that M0 and M2 macrophages along with neutrophils, were more abundant in the high-risk group (Fig. 5D). These findings suggested that a high LCaMPS score was linked to increased infiltration of neutrophils, endothelial cells, and fibroblasts in the TME, further supporting its association with an aggressive tumor phenotype in LUAD.

## Verification of the expression pattern of LCaMPS signatures

The scRNA-seq atlas revealed that 9 LCaMPS signature genes were specifically expressed in LUAD tissues, among which *SLC16A3*, *PLAUR*, and *PMEPA1* were exclusive expression in the Epi_c0 epithelial subcluster (Fig. 6A). Spatial transcriptomics further confirmed that LCaMPS signatures exhibited a strong spatial association with LUAD tumor regions across three independent samples ($R = 0.46$, $p < 0.001$ for HTA1_322_5071604; $R = 0.45$, $p < 0.001$ for HTA1_322_5071605; $R = 0.35$, $p < 0.001$ for HTA1_339_1112604; Fig. 6B, S3A, and S3C). Among the individual LCaMPS genes, *TSPAN8*, *SLC16A3*, *BACE2*, *COX16*, *PMEPA1*, and *IER3* showed consistent spatial correlations with tumor regions (all $R > 0.1$, $p < 0.001$; Fig. 6C, S3B, and S3D). *COX16* demonstrated the strongest spatial correlation with the tumor region, with R values of 0.64, 0.63, and 0.82 across the 3 LUAD tissue sections. *BACE2* and *TSPAN8* followed, with R values of 0.57, 0.46, and 0.53 for *BACE2*, and 0.43, 0.43, and 0.47 for *TSPAN8*, respectively. In the TCGA cohort, 9 LCaMPS signature genes showed significantly higher RNA expression levels in LUAD samples than in normal samples (Fig. 7A). Furthermore, protein expression

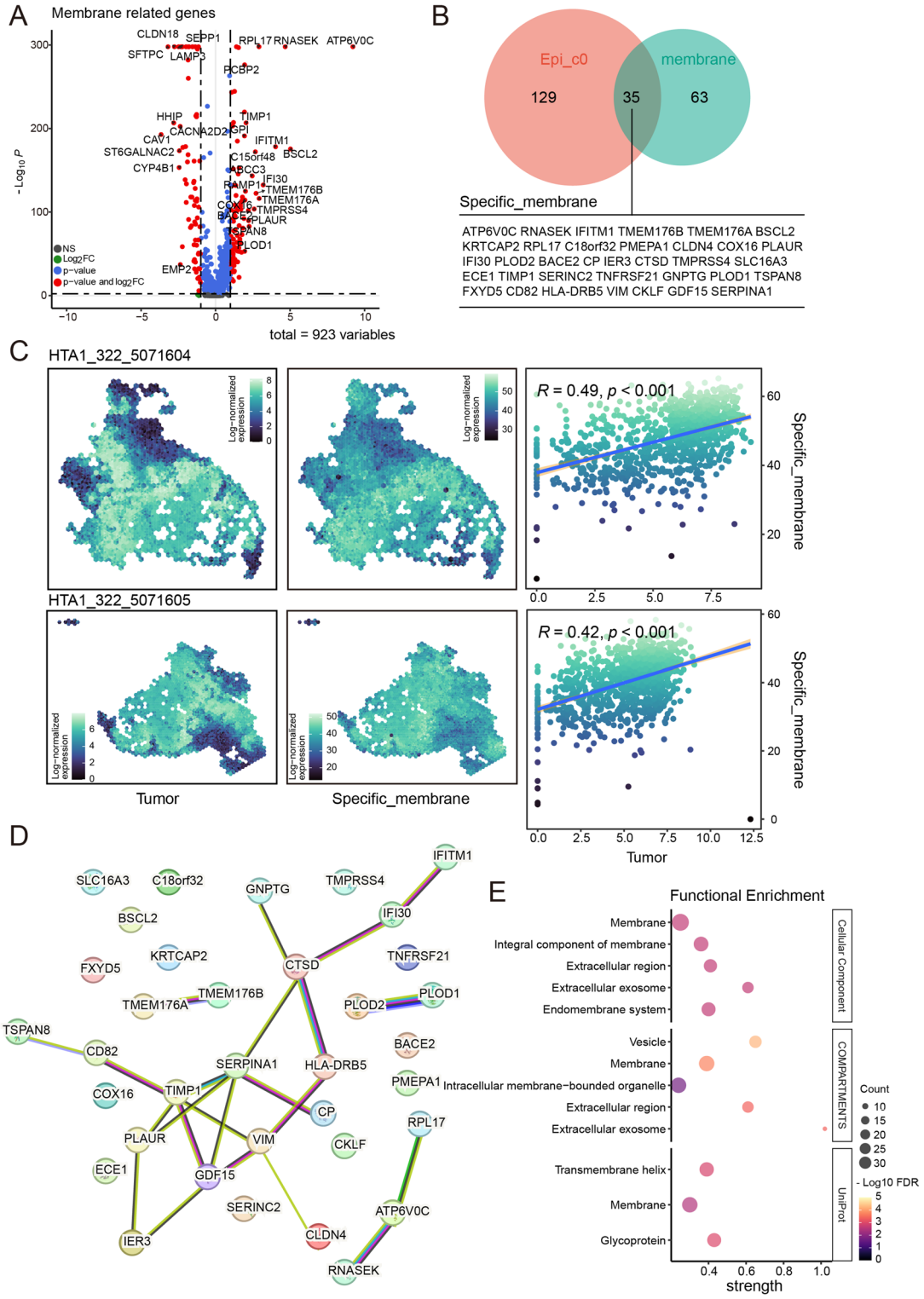


**Fig. 3**. Cancer specific membrane gene analysis of epithelial cell cluster c0. (**A**) Volcano plot illustrating the expression of 923 membrane-associated genes in LUAD compared to ADJ tissues. (**B**) Venn plot illustrating the intersection of highly expressed genes in epithelial cell cluster c0 and highly expressed membrane-associated genes in LUAD. (**C**) Spatial representation of tumor, cancer associated specific membrane and their correlations in 2 LUAD samples, top, HTA1_322_5071604; bottom, HTA1_322_5071605 from HTAN database. (**D**) The protein-protein interaction (PPI) network of 35 membrane-associated genes via STRING. (**E**) Barplot illustrating the functional enrichment of gene ontology (GO) cellular component terms, COMPARTMENTS and UniPort pathways associated with 35 membrane proteins.

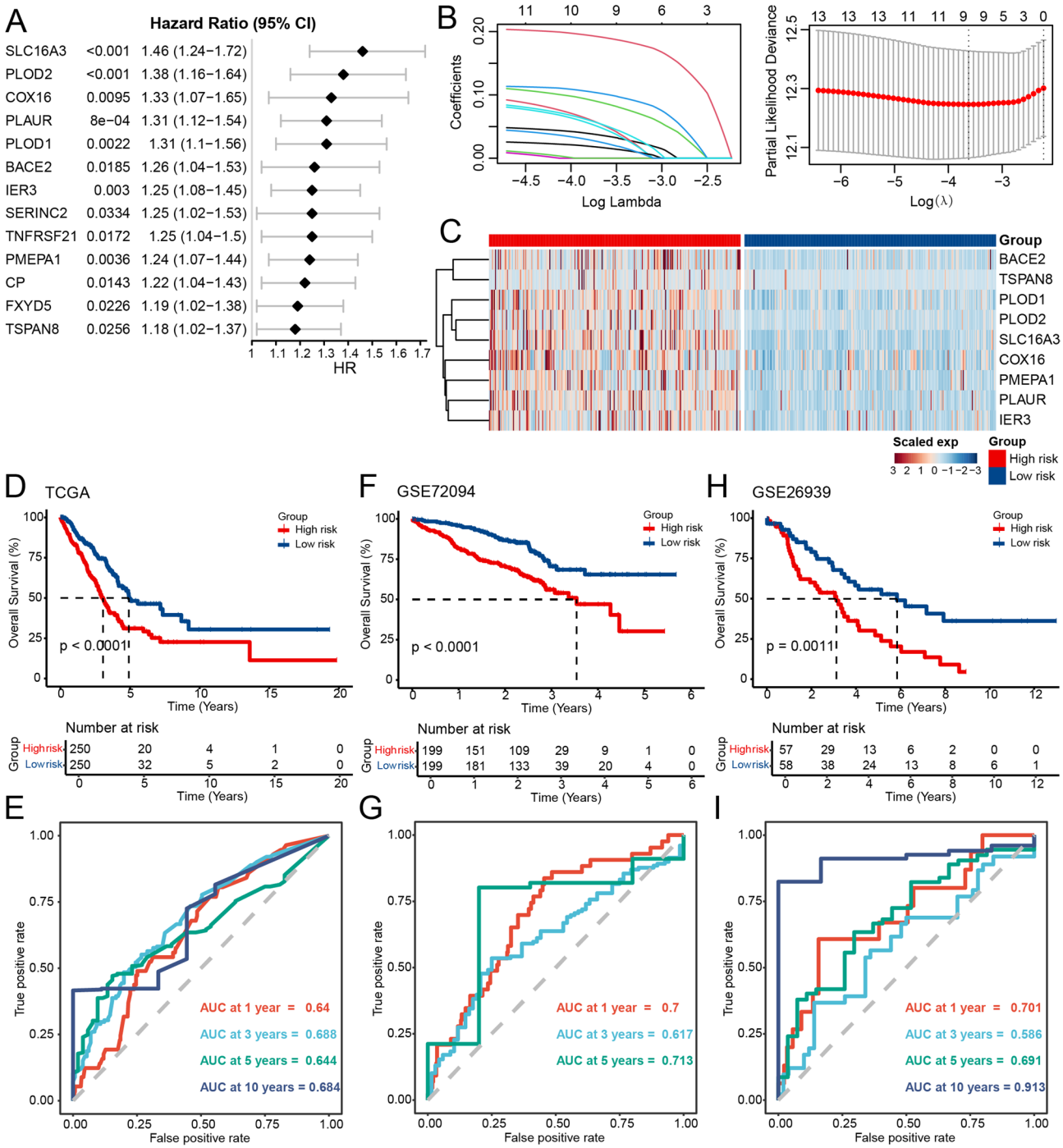


**Fig. 4**. Prognostic model of lung cancer-associated membranes (LCaMPS). (**A**) Forest plot of 13 membrane-associated genes significantly associated with prognosis of LUAD patients. (**B**) Each independent variable's trajectory and distributions for the lambda. (**C**) Heatmap showing the expression of 9 signatures in high and low-risk groups. (**D**) Kaplan-Meier plot of LCaMPS in the TCGA dataset. (**E**) The ROC curve and area under the curve (AUC) of the 1, 3, 5, and 10-years survival rates based on TCGA dataset. (**F**) Kaplan-Meier plot of LCaMPS in the validation GSE72094 cohort. (**G**) The ROC curve and AUC of the 1, 3, and 5-years survival rates based on GSE72094 cohort. (**H**) Kaplan-Meier plot of LCaMPS in the validation GSE26939 cohort. (**I**) The ROC curve and AUC of the 1, 3, 5, and 10-years survival rates based on GSE26939 cohort.

data retrieved from the THPA database demonstrated differential staining intensities among the 8 LCaMPS signature proteins in LUAD versus normal lung tissues (Fig. 7B). Specifically, *TSPAN8*, *SLC16A3*, *IER3*, and *PLAUR* showed high staining intensity in LUAD tissues, while their expression in normal lung tissues was either undetectable or low. *PLOD1*, *BACE2*, and *PLOD2* displayed low to moderate staining in LUAD, with no detectable expression in normal tissues. Notably, *COX16* showed no detectable staining in LUAD tissues

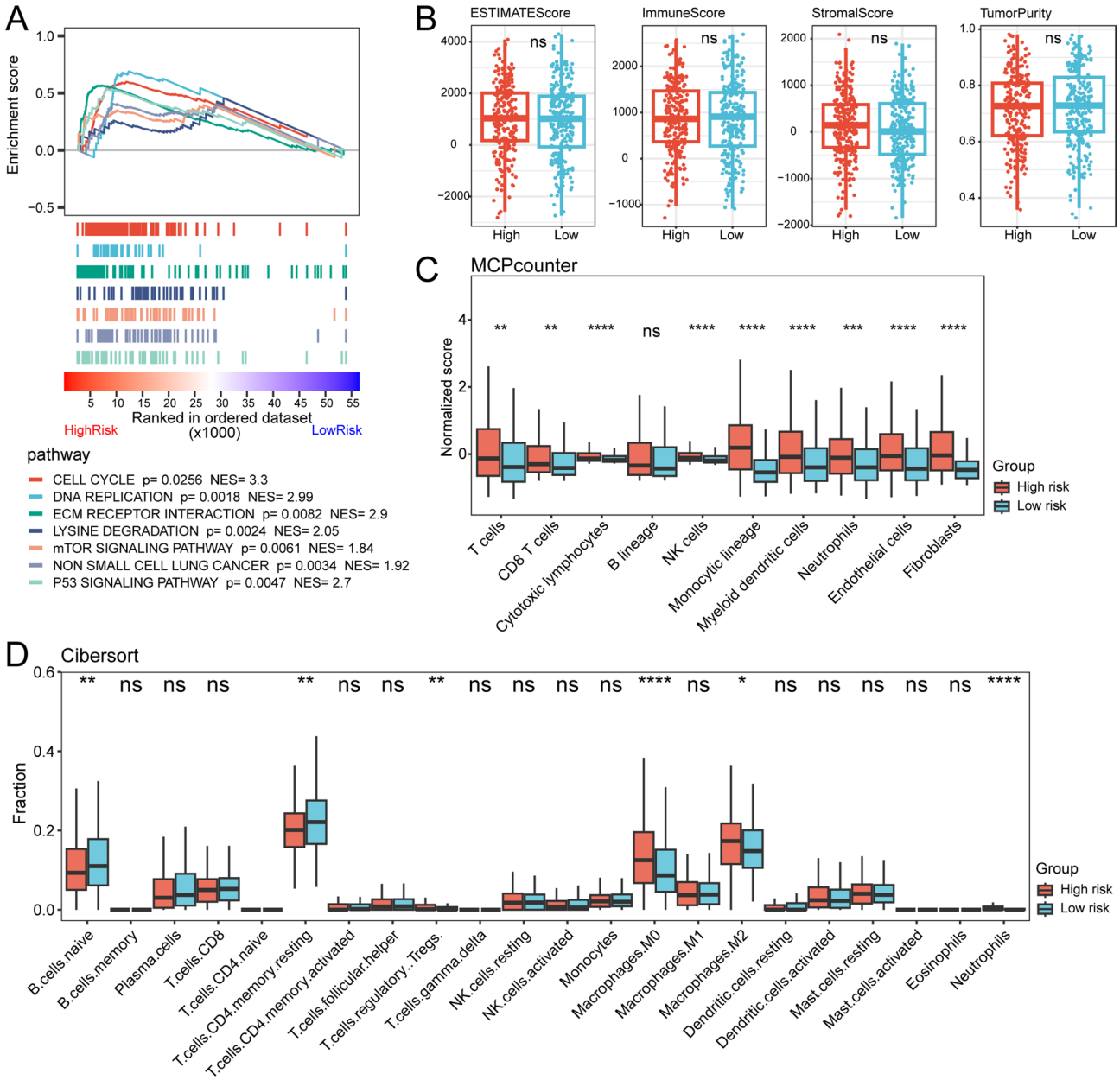


**Fig. 5**. Functional enrichment and immune cell infiltration of LCaMPS. (**A**) GSEA plot depicting KEGG pathway[21] enrichment in high and low-risk groups based on the TCGA database. (**B**) Boxplot showing ESTIMATE score, immune score, stromal score, and tumor purity between high-risk and low-risk groups. (**C**) Boxplot illustrating tissue-infiltrating immune and stromal cell populations based on MCP-counter. (**D**) Boxplot illustrating tissue-infiltrating immune cell types based on Cibersort.

and only low intensity in normal lung tissues (Fig. 7B). These findings validated that the expression profiles of LCaMPS signatures are markedly correlated with LUAD-specific tumorigenic features.

## LCaMPS exhibits predictive power for drug treatment response in LUAD

Membrane proteins play crucial roles in drug design and resistance[27,28]. To evaluate the clinical relevance of LCaMPS in therapeutic decision making, we investigated its association with drug sensitivity in LUAD. In total, the predicted responses to 138 anti-cancer drugs were analyzed. Remarkably, the LCaMPS scores were significantly correlated with the estimated IC50 values for 95 compounds (Table S5), indicating strong potential for guiding treatment selection. Among these, 66 drugs—including Docetaxel, Doxorubicin, Epothilone B, Etoposide, Gemcitabine, Obatoclax Mesylate, Paclitaxel, Vinorelbine, Tipifarnib, Thapsigargin, Sunitinib, and Sorafenib—showed lower predicted IC50 values in the high-risk group, indicating higher drug sensitivity (Fig. 8A, Table S5). In contrast, 29 drugs, including Axitinib, Camptothecin, Cisplatin, and Parthenolide, showed

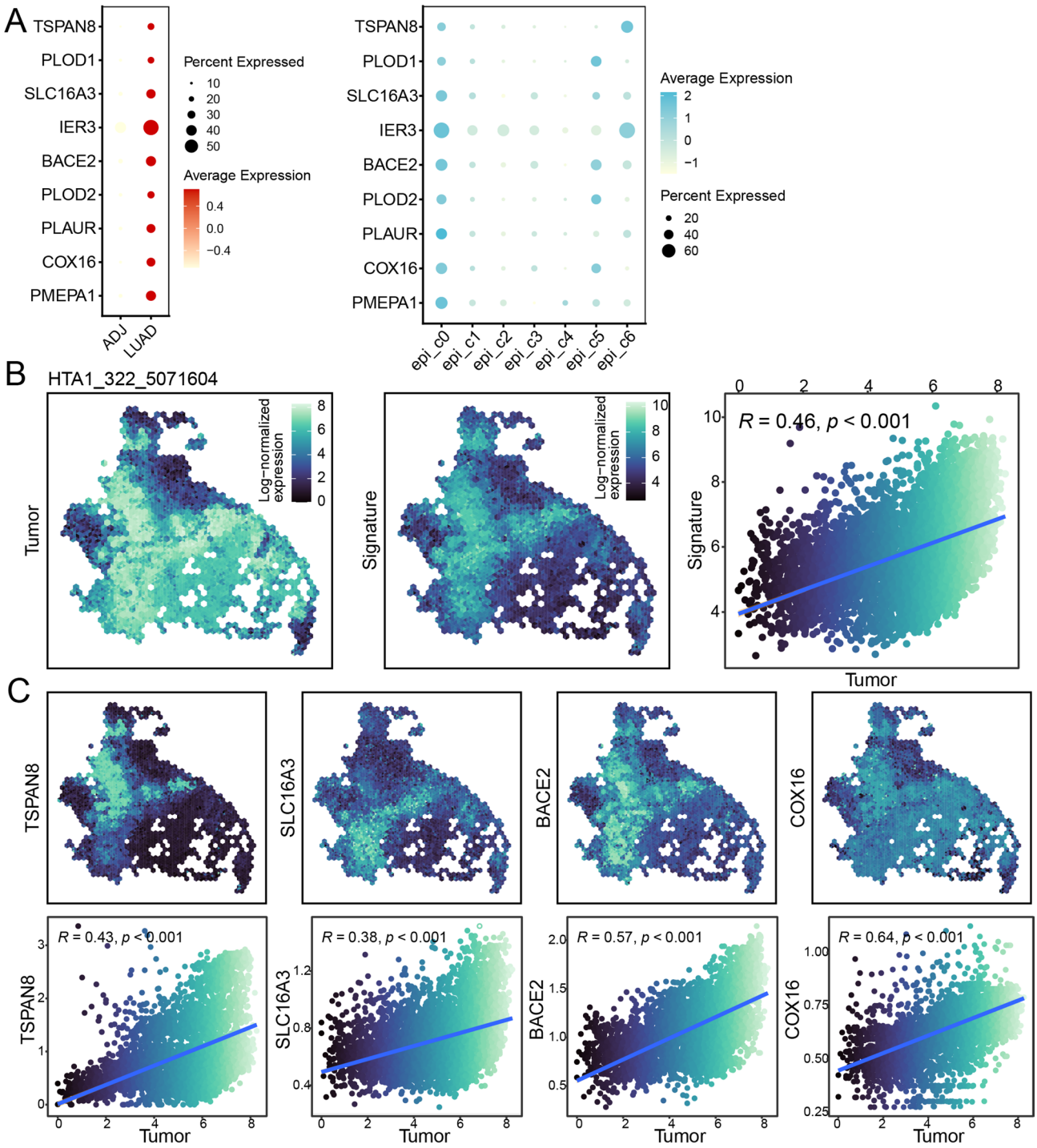


**Fig. 6**. scRNA and spatial profiling analysis of LCaMPS targets. (**A**) Dotplot illustrating the expression of the 9 signatures of LCaMPS across 2 tissue types (left) and 7 epithelial clusters (right). (**B**) Spatial representation of tumor, LCaMPS signature score and their correlation in 1 LUAD sample HTA1_322_5071604. (**C**) Spatial plot of LCaMPS signature genes, TSPAN8, SLC16A3, BACE2, COX16 and their correlations with tumor in 1 LUAD sample HTA1_322_5071604, respectively.

lower IC50 values in the low-risk group (Fig. 8B, Table S5). These results demonstrated that LCaMPS possesses predictive power for drug response and may aid in optimizing personalized treatment strategies in LUAD.

## Discussion

In this study, by integrating scRNA-seq data from multiple LUAD cohorts, we identified a distinct epithelial subpopulation characterized by cancer-associated phenotypes such as hypoxia, EMT, and the p53 signaling

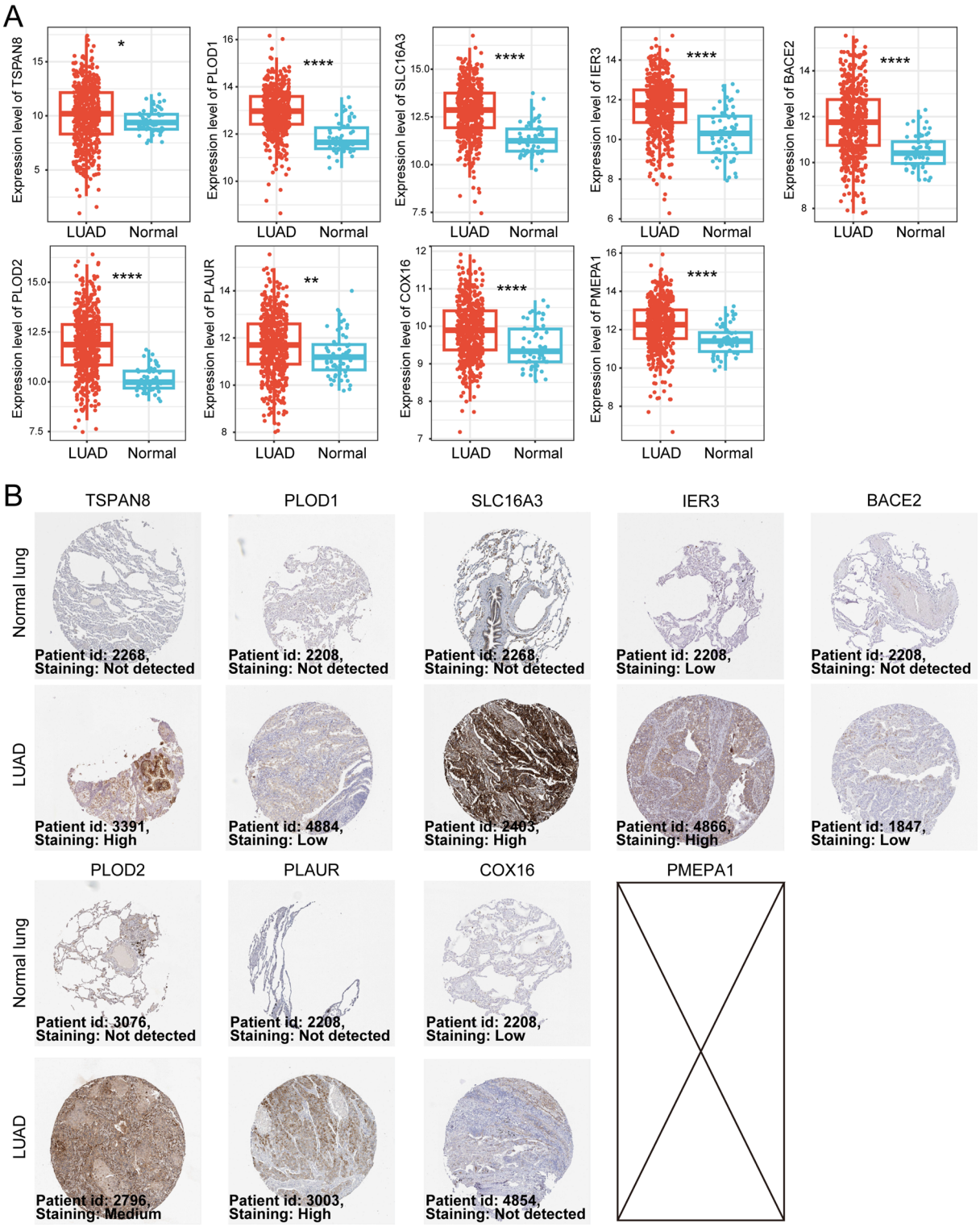


**Fig. 7**. Bulk RNA and protein profiling analysis of LCaMPS targets. (**A**) Boxplot illustrating normalized (log2 (expression + 1)) gene expression of 9 signatures of LCaMPS based on TCGA database. (**B**) Protein expression of the 8 LCaMPS signatures in LUAD and normal lung tissues via the human protein atlas (THPA). The IHC staining levels was categorized as "Not detected", "Low", "Medium", or "High".

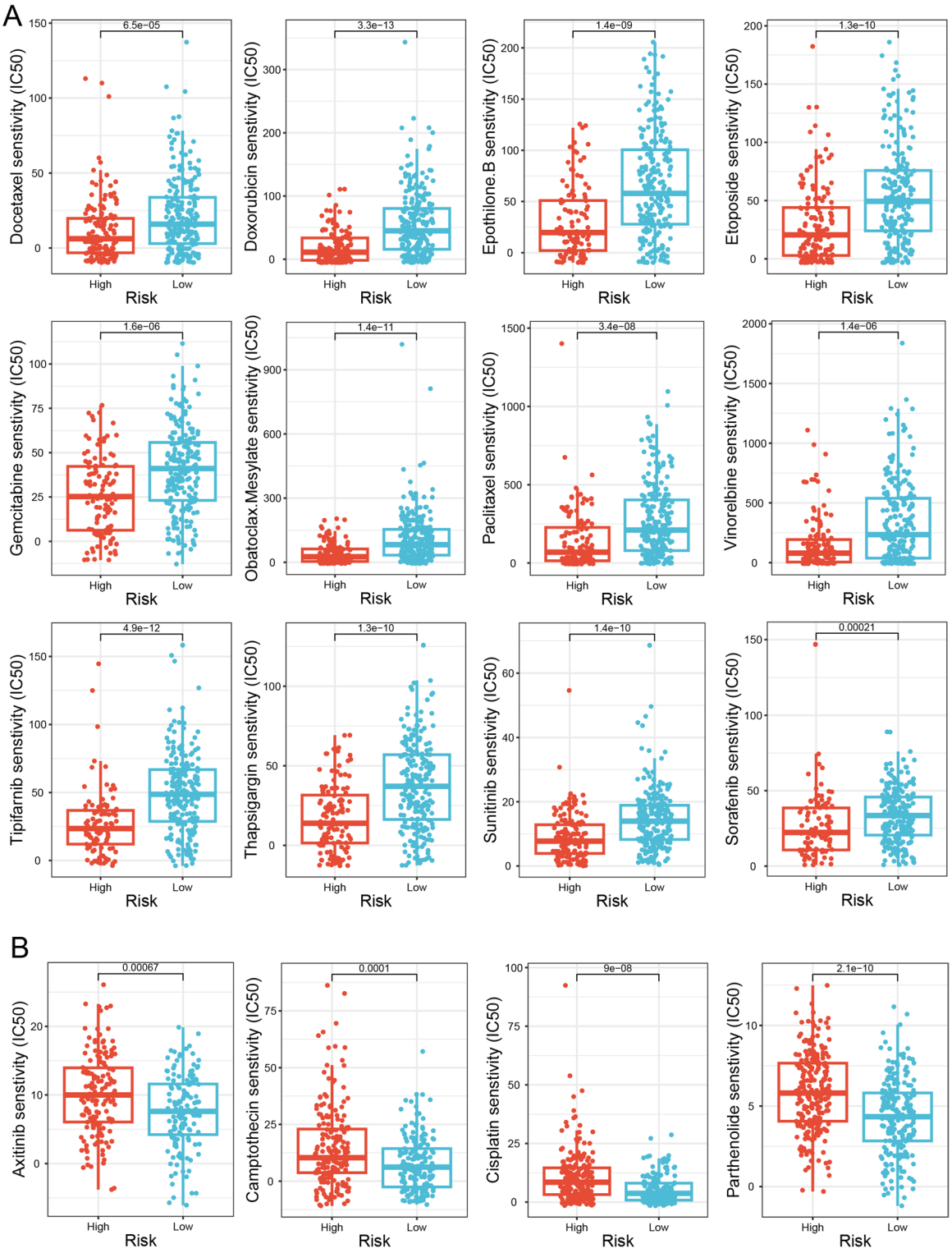


**Fig. 8**. LCaMPS associated with drug sensitivity in lung cancer. (**A**) The boxplot showing that the 12 drugs with significantly lower IC50 values in the high-risk group. (**B**) The boxplot showing that the 4 drugs with significantly lower IC50 values in the low-risk group.

pathway. A total of 35 cancer-specific membrane proteins exhibiting strong spatial association with LUAD tumor regions were identified. Based on these membrane genes, we developed a prognostic signature, LCaMPS, which stratifies patient prognosis, reflects TME patterns, and predicts potential therapeutic responses.

Cancer cells exploit hypoxic conditions to promote angiogenesis, EMT, immune evasion, and metastatic dissemination[29]. The epithelial cell cluster Epi_c0 was enriched in the hypoxia and EMT-related pathways. EMT

is a fundamental mechanism underlying immune suppression, drug resistance, and metastasis in epithelial malignancies[30]. A recent study reported that EMT activation facilitates LUAD invasion and contributes to CD8 + T cell exhaustion within the TME[31]. In addition, mutations in the tumor suppressor gene *TP53* occur in approximately 50% of LUAD cases[32]. These findings are consistent with our results and further support the notion that epithelial subpopulation Epi_c0 exhibits cancer-associated phenotypes.

Based on the membrane genes highly expressed in the Epi_c0 cluster of LUAD, we developed the LCaMPS signature. This model demonstrated favorable prognostic performance in predicting 1-, 5-, and 10-year survival, although its ability to predict 3-year survival was relatively limited. A previously published tumor stem cell-based signature (TSCMS) achieved average AUCs of 0.704, 0.652, and 0.660 for 1-, 3-, and 5-year survival in the validation cohort (with no available 10-year value), respectively[33]. our LCaMPS model exhibited superior performance at 5 and 10 years, with AUCs of 0.702 and 0.913, respectively. However, the LCaMPS scores for 1- and 3-year predictions (AUCs of 0.700 and 0.602) were not higher than the AUC of TSCMS. Moreover, a recent study proposed a prognostic model based on B cell-related genes (BRGs), which reported AUCs of 0.636, 0.591, and 0.631 for 1-, 3-, and 5-year survival, respectively (10-year unavailable)[34]. Notably, LCaMPS demonstrated a consistently better predictive performance than the BRG-based signature across all available time points in the validation cohort.

The LCaMPS model comprised 9 membrane-associated genes, all of which were found to be significantly upregulated in LUAD samples compared to adjacent normal lung tissues at the bulk RNA level. Among them, TSPAN8, SLC16A3, BACE2, COX16, PMEPA1, and IER3 exhibited strong spatial correlations with the LUAD tumor regions. While COX16 has not been previously reported in LUAD, one study identified its upregulation in oral squamous cell carcinoma (OSCC), which was associated with mitochondrial energy metabolism[35]. Suppression of COX16 expression reduced OSCC cell proliferation and metastasis[35]. TSPAN8 has been implicated in the regulation of cancer stemness-associated gene expression and resistance to therapy[36]. It functions as a key organizer of the plasma membrane and participates in cell adhesion, migration, invasion, signal transduction, and exosome biogenesis, thereby playing an oncogenic role in tumor progression and metastasis[37]. Furthermore, BACE2 has been shown to regulate NF-κB signaling; its knockout led to NF-κB inactivation and significantly inhibited glioma stem cell (GSC) tumorigenesis and radioresistance[38]. These findings are consistent with our results and suggest that LCaMPS may serve as a prognostic biomarker and potential target framework for guiding personalized therapeutic interventions in LUAD.

Functionally, the LCaMPS risk score was associated with cancer cell proliferation and migration, as indicated by its enrichment in pathways such as the cell cycle, DNA replication, and ECM-receptor interaction. Cancer cells often exhibit uncontrolled cell cycle progression. In tumors, cell cycle-dependent DNA repair and replication have been linked to focal mutagenesis in multiple cancer types[39–41]. A recent study also reported that dysregulation of ECM-receptor interactions contributes to enhanced migration and invasion in LUAD[42]. These findings suggest that patients with high LCaMPS scores may harbor tumor cells with proliferative potential and an increased invasive capacity. Moreover, neutrophils are recognized as key modulators in cancer, and their functionality within the TME is highly diverse; they may be reprogrammed into a pro-tumorigenic state[43,44]. Cancer-associated endothelial cells and fibroblasts have been implicated in promoting cancer proliferation and invasion in several cancer types[45–48]. Our results further indicated that a high LCaMPS score was linked to increased infiltration of neutrophils, endothelial cells, and fibroblasts in the TME, underscoring the potential role of LCaMPS in delineating aggressive tumor behavior. Furthermore, recent studies have further underscored the importance of the TME in modulating immune responses and shaping tumor progression[49–51]. Membrane-associated molecules such as B4GALT2 were identified as key mediators of immune exclusion, particularly by depleting CD8 + T cells within the LUAD TME[50]. Another integrated multi-omics study has identified immune-evasive drivers such as CEP55, which regulate T cell dysfunction and immunotherapy resistance. These findings support that cancer-associated membranes, such as those identified in LCaMPS, may participate in shaping the TME landscape of LUAD and hold promise for refining immunotherapeutic strategies.

We evaluated the potential of LCaMPS in predicting drug treatment responses in patients with LUAD. Patients with high-LCaMPS were predicted to be more sensitive to 66 chemotherapeutic agents, including Paclitaxel, Docetaxel, Gemcitabine, Vinorelbine, and Sorafenib. Both Paclitaxel and Docetaxel have long been used as frontline chemotherapeutic agents for NSCLC treatment[52]. Gemcitabine is an FDA-approved nucleoside analog used for the treatment of various malignancies, including breast cancer, lung cancer, pancreatic cancer, and ovarian cancer, owing to its broad applicability and relatively low toxicity[53,54]. A recent randomized phase II clinical trial demonstrated that vinorelbine offered a clinically meaningful improvement in OS as an adjuvant therapy for NSCLC[55]. Notably, Sorafenib has shown therapeutic potential in NSCLC cell lines, xenograft models, and early-phase clinical trials involving human subjects[56]. These observations suggest that patients with high LCaMPS scores may benefit from prioritizing these agents during chemotherapy. In contrast, patients with low LCaMPS scores were predicted to be more sensitive to 29 other compounds including Cisplatin and Parthenolide. Cisplatin remains one of the most commonly used adjuvant chemotherapy agents for NSCLC, and cisplatin-based regimens have been shown to improve OS[57]. Although Parthenolide is yet to enter clinical trials for lung cancer, it has been shown to inhibit NF-κB signaling and other pro-survival pathways, induce apoptosis, and reduce the viability of multiple cancer cell types in preclinical studies[58–60]. Thus, these findings support our assessment of drug sensitivity and highlight the potential of LCaMPS as a predictive biomarker for guiding personalized chemotherapy regimens in LUAD.

However, several limitations should be acknowledged. First, although the LCaMPS was validated across multiple independent cohorts, all data were derived from public databases, and the conclusions have not yet been confirmed in prospective clinical settings. Second, our drug therapeutic response predictions were computationally derived and will benefit from future pharmacological validation. Third, protein-level expression

was explored using standardized public IHC data; however, real-world confirmation would further strengthen the translational relevance.

Future studies should aim to validate the LCaMPS model in clinical trial cohorts, and exploring its predictive potential across diverse LUAD subtypes and therapeutic contexts. Functional studies of selected signature genes, including COX16, TSPAN8, and BACE2, may uncover novel mechanisms of tumor progression and immune modulation. Taken together, despite these considerations, LCaMPS provides a promising prognostic tool that offers valuable insights for advancing precision oncology in LUAD.

## Conclusion

In conclusion, we developed a novel LUAD-specific membrane-based prognostic signature, LCaMPS, by integrating scRNA-seq, spatial transcriptomic, and bulk RNA-seq datasets. LCaMPS not only stratifies patient prognosis with long-term predictive value but also reflects key features of the TME and indicates potential responsiveness to multiple chemotherapeutic agents. Taken together, our findings suggest that LCaMPS has strong potential as a biomarker for both prognostic stratification and personalized therapeutic guidance in LUAD.

## Data availability

scRNA-seq data can be accessed from GEO under accession numbers GSE117570[8], GSE131907[7], GSE164983, and GSE274934[6], and spatial transcriptomics data from HTAN. Bulk RNA-seq and clinical information can be obtained from the TCGA-LUAD cohort, and GEO under accession number GSE26939[13] and GSE72094[14]. For any other reasonable requests, please contact the corresponding author.

## Code availability

The relevant code used in this study will be made available upon request.

Received: 27 April 2025; Accepted: 8 July 2025
Published online: 15 July 2025

## References

1. Sung, H. et al. Global Cancer statistics 2020: GLOBOCAN estimates of incidence and mortality worldwide for 36 cancers in 185 countries. *CA Cancer J. Clin.* **71**, 209–249. https://doi.org/10.3322/caac.21660 (2021).
2. Ferlay, J. et al. Cancer incidence and mortality patterns in europe: estimates for 40 countries and 25 major cancers in 2018. *Eur. J. Cancer* **103**, 356–387. https://doi.org/10.1016/j.ejca.2018.07.005 (2018).
3. Kerdidani, D. et al. Wnt1 silences chemokine genes in dendritic cells and induces adaptive immune resistance in lung adenocarcinoma. *Nat. Commun.* **10**, 1405. https://doi.org/10.1038/s41467-019-09370-z (2019).
4. Herbst, R. S., Morgensztern, D. & Boshoff, C. The biology and management of non-small cell lung cancer. *Nature* **553**, 446–454. https://doi.org/10.1038/nature25183 (2018).
5. Hirsch, F. R. et al. Lung cancer: current therapies and new targeted treatments. *Lancet* **389**, 299–311. https://doi.org/10.1016/s0140-6736(16)30958-8 (2017).
6. Baek, S. et al. Single-cell multi-omics reveals tumor microenvironment factors underlying poor immunotherapy responses in ALK-positive lung cancer. *Cancer Commun. (Lond)*. https://doi.org/10.1002/cac2.12658 (2025).
7. Kim, N. et al. Single-cell RNA sequencing demonstrates the molecular and cellular reprogramming of metastatic lung adenocarcinoma. *Nat. Commun.* **11**, 2285. https://doi.org/10.1038/s41467-020-16164-1 (2020).
8. Song, Q. et al. Dissecting intratumoral myeloid cell plasticity by single cell RNA-seq. *Cancer Med.* **8**, 3072–3085. https://doi.org/10.1002/cam4.2113 (2019).
9. De Zuani, M. et al. Single-cell and Spatial transcriptomics analysis of non-small cell lung cancer. *Nat. Commun.* **15**, 4388. https://doi.org/10.1038/s41467-024-48700-8 (2024).
10. Yong, C. Q. Y. & Tang, B. L. Cancer-driving mutations and variants of components of the membrane trafficking core machinery. *Life Sci.* **264**, 118662. https://doi.org/10.1016/j.lfs.2020.118662 (2021).
11. Gounou, C. et al. Inhibition of the membrane repair protein annexin-A2 prevents tumor invasion and metastasis. *Cell. Mol. Life Sci.* **81**, 7. https://doi.org/10.1007/s00018-023-05049-3 (2023).
12. Chen, C. et al. Single-cell and Spatial transcriptomics reveal POSTN(+) cancer-associated fibroblasts correlated with immune suppression and tumour progression in non-small cell lung cancer. *Clin. Transl Med.* **13**, e1515. https://doi.org/10.1002/ctm2.1515 (2023).
13. Wilkerson, M. D. et al. Differential pathogenesis of lung adenocarcinoma subtypes involving sequence mutations, copy number, chromosomal instability, and methylation. *PLoS One*. **7**, e36530. https://doi.org/10.1371/journal.pone.0036530 (2012).
14. Schabath, M. B. et al. Differential association of STK11 and TP53 with KRAS mutation-associated gene expression, proliferation and immune surveillance in lung adenocarcinoma. *Oncogene* **35**, 3209–3216. https://doi.org/10.1038/onc.2015.375 (2016).
15. Butler, A., Hoffman, P., Smibert, P., Papalexi, E. & Satija, R. Integrating single-cell transcriptomic data across different conditions, technologies, and species. *Nat. Biotechnol.* **36**, 411–420. https://doi.org/10.1038/nbt.4096 (2018).
16. Korsunsky, I. et al. Fast, sensitive and accurate integration of single-cell data with harmony. *Nat. Methods*. **16**, 1289–1296. https://doi.org/10.1038/s41592-019-0619-0 (2019).
17. Zhao, E. et al. Spatial transcriptomics at Subspot resolution with bayesspace. *Nat. Biotechnol.* **39**, 1375–1384. https://doi.org/10.1038/s41587-021-00935-2 (2021).
18. Hu, C. et al. CellMarker 2.0: an updated database of manually curated cell markers in human/mouse and web tools based on scRNA-seq data. *Nucleic Acids Res.* **51**, D870–d876. https://doi.org/10.1093/nar/gkac947 (2023).
19. Szklarczyk, D. et al. The STRING database in 2023: protein-protein association networks and functional enrichment analyses for any sequenced genome of interest. *Nucleic Acids Res.* **51**, D638–d646. https://doi.org/10.1093/nar/gkac1000 (2023).
20. Liberzon, A. et al. The molecular signatures database (MSigDB) hallmark gene set collection. *Cell. Syst.* **1**, 417–425. https://doi.org/10.1016/j.cels.2015.12.004 (2015).
21. Kanehisa, M., Sato, Y., Kawashima, M., Furumichi, M. & Tanabe, M. KEGG as a reference resource for gene and protein annotation. *Nucleic Acids Res.* **44**, D457–462. https://doi.org/10.1093/nar/gkv1070 (2016).
22. Kanehisa, M. & Goto, S. KEGG: Kyoto encyclopedia of genes and genomes. *Nucleic Acids Res.* **28**, 27–30. https://doi.org/10.1093/nar/28.1.27 (2000).

23. Becht, E. et al. Estimating the population abundance of tissue-infiltrating immune and stromal cell populations using gene expression. *Genome Biol.* **17**, 218. https://doi.org/10.1186/s13059-016-1070-5 (2016).
24. Chen, B., Khodadoust, M. S., Liu, C. L., Newman, A. M. & Alizadeh, A. A. Profiling tumor infiltrating immune cells with CIBERSORT. *Methods Mol. Biol.* **1711**, 243–259. https://doi.org/10.1007/978-1-4939-7493-1_12 (2018).
25. Colwill, K. & Gräslund, S. A roadmap to generate renewable protein binders to the human proteome. *Nat. Methods.* **8**, 551–558. https://doi.org/10.1038/nmeth.1607 (2011).
26. Geeleher, P., Cox, N. & Huang, R. S. pRRophetic: an R package for prediction of clinical chemotherapeutic response from tumor gene expression levels. *PLoS One.* **9**, e107468. https://doi.org/10.1371/journal.pone.0107468 (2014).
27. Jiang, Y. et al. Targeting extracellular matrix stiffness and mechanotransducers to improve cancer therapy. *J. Hematol. Oncol.* **15** https://doi.org/10.1186/s13045-022-01252-0 (2022).
28. Jaakola, V. P. & Scalise, M. Membrane proteins: new approaches to probes, technologies, and drug design, part II. *SLAS Discov.* **24**, 941–942. https://doi.org/10.1177/2472555219881666 (2019).
29. Wicks, E. E. & Semenza, G. L. Hypoxia-inducible factors: cancer progression and clinical translation. *J. Clin. Invest.* **132** https://doi.org/10.1172/jci159839 (2022).
30. Rodriguez-Boulan, E. & Macara, I. G. Organization and execution of the epithelial Polarity programme. *Nat. Rev. Mol. Cell. Biol.* **15**, 225–242. https://doi.org/10.1038/nrm3775 (2014).
31. Xiao, G. Y. et al. EMT activates exocytotic Rabs to coordinate invasion and immunosuppression in lung cancer. *Proc. Natl. Acad. Sci. U S A.* **120**, e2220276120. https://doi.org/10.1073/pnas.2220276120 (2023).
32. Kaiser, A. M. et al. p53 governs an AT1 differentiation programme in lung cancer suppression. *Nature* **619**, 851–859. https://doi.org/10.1038/s41586-023-06253-8 (2023).
33. Zhao, F., Chen, M., Wu, T., Ji, M. & Li, F. Integration of single-cell and bulk RNA sequencing to identify a distinct tumor stem cells and construct a novel prognostic signature for evaluating prognosis and immunotherapy in LUAD. *J. Transl Med.* **23**, 222. https://doi.org/10.1186/s12967-025-06243-6 (2025).
34. Xu, K. et al. B-cell signatures characterize the immune landscape and predict LUAD prognosis via the integration of scRNA-seq and bulk RNA-seq. *Sci. Rep.* **15**, 5453. https://doi.org/10.1038/s41598-025-89213-8 (2025).
35. Zhang, J. et al. DAZAP1 phase separation regulates mitochondrial metabolism to facilitate invasion and metastasis of oral squamous cell carcinoma. *Cancer Res.* **84**, 3818–3833. https://doi.org/10.1158/0008-5472.Can-24-0067 (2024).
36. Zhu, R. et al. TSPAN8 promotes cancer cell stemness via activation of Sonic Hedgehog signaling. *Nat. Commun.* **10**, 2863. https://doi.org/10.1038/s41467-019-10739-3 (2019).
37. Yang, J., Zhang, Z., Lam, J. S. W., Fan, H. & Fu, N. Y. Molecular regulation and oncogenic functions of TSPAN8. *Cells* **13**, https://doi.org/10.3390/cells13020193 (2024).
38. Chen, Z. et al. Cell surface GRP78 regulates BACE2 via lysosome-dependent manner to maintain mesenchymal phenotype of glioma stem cells. *J. Exp. Clin. Cancer Res.* **40** https://doi.org/10.1186/s13046-020-01807-4 (2021).
39. Matthews, H. K., Bertoli, C. & de Bruin, R. A. M. Cell cycle control in cancer. *Nat. Rev. Mol. Cell. Biol.* **23**, 74–88. https://doi.org/10.1038/s41580-021-00404-3 (2022).
40. Murat, P., Guilbaud, G. & Sale, J. E. DNA replication initiation drives focal mutagenesis and rearrangements in human cancers. *Nat. Commun.* **15**, 10850. https://doi.org/10.1038/s41467-024-55148-3 (2024).
41. Lu, B., Winnall, S., Cross, W. & Barnes, C. P. Cell-cycle dependent DNA repair and replication unifies patterns of chromosome instability. *Nat. Commun.* **16**, 3033. https://doi.org/10.1038/s41467-025-58245-z (2025).
42. Yang, L., Shen, A., Wang, R. & Zheng, Z. S100A16 stabilizes the ITGA3–mediated ECM–receptor interaction pathway to drive the malignant properties of lung adenocarcinoma cells via binding MOV10. *Mol. Med. Rep.* **31** https://doi.org/10.3892/mmr.2024.13376 (2025).
43. Hedrick, C. C. & Malanchi, I. Neutrophils in cancer: heterogeneous and multifaceted. *Nat. Rev. Immunol.* **22**, 173–187. https://doi.org/10.1038/s41577-021-00571-6 (2022).
44. Xiong, S., Dong, L. & Cheng, L. Neutrophils in cancer carcinogenesis and metastasis. *J. Hematol. Oncol.* **14**, 173. https://doi.org/10.1186/s13045-021-01187-y (2021).
45. Wu, J. et al. Characterization of tumor-associated endothelial cells and the development of a prognostic model in pancreatic ductal adenocarcinoma. *Biochim. Biophys. Acta Gen. Subj.* **1868**, 130545. https://doi.org/10.1016/j.bbagen.2023.130545 (2024).
46. Cords, L. et al. Cancer-associated fibroblast phenotypes are associated with patient outcome in non-small cell lung cancer. *Cancer Cell.* **42**, 396–412e395. https://doi.org/10.1016/j.ccell.2023.12.021 (2024).
47. Li, X. et al. Single-cell RNA sequencing reveals a pro-invasive cancer-associated fibroblast subgroup associated with poor clinical outcomes in patients with gastric cancer. *Theranostics* **12**, 620–638. https://doi.org/10.7150/thno.60540 (2022).
48. Lu, Y. et al. CXCL12(+) tumor-associated endothelial cells promote immune resistance in hepatocellular carcinoma. *J. Hepatol.* **82**, 634–648. https://doi.org/10.1016/j.jhep.2024.09.044 (2025).
49. Ye, B. et al. Navigating the immune landscape with plasma cells: A pan-cancer signature for precision immunotherapy. *Biofactors* **51**, e2142. https://doi.org/10.1002/biof.2142 (2025).
50. Zhang, P. et al. Novel post-translational modification learning signature reveals B4GALT2 as an immune exclusion regulator in lung adenocarcinoma. *J. Immunother Cancer* **13** https://doi.org/10.1136/jitc-2024-010787 (2025).
51. Ye, B. et al. iMLGAM: integrated machine learning and genetic Algorithm-driven multiomics analysis for pan-cancer immunotherapy response prediction. *Imeta* **4**, e70011. https://doi.org/10.1002/imt2.70011 (2025).
52. Francis, P. A., Kris, M. G., Rigas, J. R., Grant, S. C. & Miller, V. A. Paclitaxel (Taxol) and docetaxel (Taxotere): active chemotherapeutic agents in lung cancer. *Lung Cancer.* **12** (Suppl 1), S163–172. https://doi.org/10.1016/0169-5002(95)00432-z (1995).
53. Larson, A. C., Doty, K. R. & Solheim, J. C. The double life of a chemotherapy drug: Immunomodulatory functions of gemcitabine in cancer. *Cancer Med.* **13**, e7287. https://doi.org/10.1002/cam4.7287 (2024).
54. Zhang, X. et al. Low-Dose gemcitabine treatment enhances immunogenicity and natural killer Cell-Driven tumor immunity in lung Cancer. *Front. Immunol.* **11**, 331. https://doi.org/10.3389/fimmu.2020.00331 (2020).
55. Yue, D. et al. Updated overall survival and exploratory analysis from randomized, phase II EVAN study of erlotinib versus Vinorelbine plus cisplatin adjuvant therapy in stage IIIA epidermal growth factor Receptor + Non-Small-Cell lung Cancer. *J. Clin. Oncol.* **40**, 3912–3917. https://doi.org/10.1200/jco.22.00428 (2022).
56. Hendrixson, M., Gladkiy, Y., Thyagarajan, A. & Sahu, R. P. Efficacy of sorafenib-based therapies for non-small cell lung cancer. *Med. Sci. (Basel)* **12** https://doi.org/10.3390/medsci12020020 (2024).
57. Arriagada, R. et al. Cisplatin-based adjuvant chemotherapy in patients with completely resected non-small-cell lung cancer. *N Engl. J. Med.* **350**, 351–360. https://doi.org/10.1056/NEJMoa031644 (2004).
58. Carlisi, D. et al. Parthenolide and DMAPT exert cytotoxic effects on breast cancer stem-like cells by inducing oxidative stress, mitochondrial dysfunction and necrosis. *Cell. Death Dis.* **7**, e2194. https://doi.org/10.1038/cddis.2016.94 (2016).
59. Flores-Lopez, G. et al. Parthenolide and DMAPT induce cell death in primitive CML cells through reactive oxygen species. *J. Cell. Mol. Med.* **22**, 4899–4912. https://doi.org/10.1111/jcmm.13755 (2018).
60. Czyz, M., Koprowska, K. & Sztiller-Sikorska, M. Parthenolide reduces the frequency of ABCB5-positive cells and clonogenic capacity of melanoma cells from anchorage independent melanospheres. *Cancer Biol. Ther.* **14**, 135–145. https://doi.org/10.4161/cbt.22952 (2013).

## Acknowledgements
We are thankful to Ms. Ying Chen for her valuable suggestions on the layout of the workflow diagram.

## Author contributions
Biao Tu: Conceptualization, Formal analysis, Visualization, Writing—original draft, Methodology. Jun Wu: Conceptualization, Supervision, Methodology, Writing—review & editing. Wei Zhang: Formal analysis, Methodology, Data curation. Haitao Tang: Data curation, Methodology, Investigation. Tenghui Dai: Data curation, Investigation. Bingfeng Xie: Conceptualization, Supervision, Resources, Writing—review & editing.

## Declarations

## Competing interests
The authors declare no competing interests.

## Additional information
**Supplementary Information** The online version contains supplementary material available at https://doi.org/10.1038/s41598-025-11105-8.

**Correspondence** and requests for materials should be addressed to J.W. or B.X.

**Reprints and permissions information** is available at www.nature.com/reprints.

**Publisher's note** Springer Nature remains neutral with regard to jurisdictional claims in published maps and institutional affiliations.